

UV photoprocessing of NH₃ ice: photon-induced desorption mechanisms

R. Martín-Doménech,¹ G. A. Cruz-Díaz,^{2,3} G. M. Muñoz Caro,⁴

¹Harvard-Smithsonian Center for Astrophysics, Cambridge, MA 02138, USA

²Bay Area Environmental Research Institute, Petaluma, CA 94952, USA

³NASA Ames Research Center, Moffet Field, Mountain View, CA 94035, USA

⁴Centro de Astrobiología (INTA-CSIC). Ctra de Ajalvir, Km. 4, Torrejón de Ardoz, 28850 Madrid, Spain

Accepted XXX. Received YYY; in original form ZZZ

ABSTRACT

Ice mantles detected on the surface of dust grains toward the coldest regions of the interstellar medium can be photoprocessed by the secondary ultraviolet (UV) field present in dense cloud interiors. In this work, we present UV-irradiation experiments under astrophysically relevant conditions of pure NH₃ ice samples in an ultra-high vacuum chamber where solid samples were deposited onto a substrate at 8 K. The ice analogs were subsequently photoprocessed with a microwave-discharged hydrogen-flow lamp. The induced radiation and photochemistry led to the production of H₂, N₂ and N₂H₄. In addition, photodesorption to the gas phase of the original ice component, NH₃, and two of the three detected photoproducts, H₂ and N₂, was observed thanks to a quadrupole mass spectrometer (QMS). Calibration of the QMS allowed quantification of the photodesorption yields, leading to $Y_{pd}(\text{NH}_3) = 2.1_{-1.0}^{+2.1} \times 10^{-3} \frac{\text{molecules}}{\text{incident photon}}$, which remained constant during the whole experiments, while photodesorption of H₂ and N₂ increased with fluence, pointing toward an indirect photodesorption mechanism involving energy transfer for these species. Photodesorption yield of N₂ molecules after a fluence equivalent to that experienced by ice mantles in space was similar to that of the NH₃ molecules ($Y_{pd}(\text{N}_2) = 1.7_{-0.9}^{+1.7} \times 10^{-3} \frac{\text{molecules}}{\text{incident photon}}$).

Key words: methods:laboratory:molecular - ISM:clouds - ISM: molecules

1 INTRODUCTION

Infrared observations, mainly performed by space telescopes like the Infrared Space Observatory (ISO), Spitzer, and AKARI, have revealed the presence of ice mantles on the surface of interstellar dust grains in dense interstellar clouds (see, e.g., Gibb et al. (2004); Öberg et al. (2011), and references therein). Water is the major component of the ice mantles, but five more species are confirmed to be present with varying abundances relative to H₂O: CO, CO₂, CH₃OH, NH₃, and CH₄; and several more have been tentatively detected (Boogert et al. (2015) and references therein).

Ice molecules are processed by cosmic rays and the secondary ultraviolet (UV) field produced in the interior of dense clouds when the cosmic rays interact with the gas-phase H₂ molecules (Cecchi-Pestellini & Aiello (1992); Shen et al. (2004)). In particular, UV photons induce photochemical reactions by photolysis of absorbing molecules and recombination of the produced radicals (see Öberg et al. (2016) and references therein), and also photodesorption processes, which represent one of the proposed non-thermal desorption

mechanisms necessary to explain the presence of gas-phase molecules in the coldest regions of the interstellar medium (ISM), where they should be completely depleted forming these ice mantles (e.g., Wilacy & Langer (2000); Bergin et al. (2001)).

Depending on whether the photodesorbing molecule is the same ice molecule that absorbs the UV photon (or at least a fragment of the molecule), or a different molecule, one can distinguish between direct photodesorption mechanisms, and photodesorption mechanisms involving energy transfer, respectively.

In the case that the photon is absorbed by a surface ice molecule that does not subsequently photodissociate, the absorbing molecule can directly photodesorb to the gas phase. This mechanism has been proposed by van Hemert et al. (2015) for the photodesorption of CO molecules from a pure CO ice based on molecular dynamics simulations. However, in previous works this process had been proven to be inefficient during experimental simulations with CO and N₂ ices when compared to indirect photodesorption mechanisms

arXiv:1710.06467v1 [astro-ph.GA] 17 Oct 2017

(see, e.g., Muñoz Caro et al. (2010); Bertin et al. (2012, 2013)), although it may have a contribution in other cases (Dupuy et al. (2017)). Alternatively, if the absorbing surface molecule photodissociates, the resulting photofragment can desorb provided that it is formed with enough kinetic energy, or it may recombine with another fragment, leading to the formation of a photoproduct that could also photodesorb thanks to the excess energy of the parent photofragments and/or the exothermicity released during the recombination reaction (see, e.g., Andersson & van Dishoeck (2008); Fayolle et al. (2013); Fillion et al. (2014); Bertin et al. (2016)). Since the direct photodesorption of photoproducts through this mechanism (which is referred to as photochemical desorption or photochemidesorption in previous works; Martín-Doménech et al. (2016); Cruz-Díaz et al. (2016)) takes place immediately after their formation, photoproducts cannot be accumulated on the ice surface prior to their photodesorption, and the measured photodesorption yield during experimental simulations remains constant with fluence.

On the other hand, if the photon is absorbed by a molecule below the ice surface leading to its electronic excitation, the energy can be redistributed or transferred to a surface molecule¹ that could break the intermolecular bonds and photodesorb. This process is usually known as desorption induced by electronic transitions (DIET) followed by subsequent energetic transfer² (Fayolle et al. (2011, 2013); Bertin et al. (2012, 2013); Fillion et al. (2014)), and it is referred to as kick-out photodesorption in van Hemert et al. (2015). In the case that the absorbing molecule dissociates, the excess energy can be transferred by the resulting photofragment to a surface molecule, leading to its photodesorption. When the photofragment is an H atom, it can diffuse through the ice and transfer its momentum to a surface molecule. This is known as kick-out photodesorption³ (Andersson & van Dishoeck (2008)). Alternatively, the excess energy from the recombination of the photofragments can also be transferred to a surface molecule leading to its photodesorption (Andersson & van Dishoeck (2008); Fillion et al. (2014)). When a previously formed photoproduct photodesorbs through any of these indirect mechanisms, accumulation in the ice prior to their photodesorption leads to an increasing photodesorption yield with fluence, as measured during experimental simulations (Martín-Doménech et al. (2015, 2016); Cruz-Díaz et al. (2016)).

Experimental simulations aiming to study the photodesorption of molecules taking place during photoprocessing of pure ices made by the six species confirmed to be present in interstellar ice mantles are a necessary first step

¹ The transfer of energy could also take place between molecules on the surface of the ice.

² The term DIET could, in principle, encompass all photodesorption processes, and does not necessarily imply energetic transfer. However these two concepts tend to be related in the literature (see Fayolle et al. (2011); Bertin et al. (2012)). In addition, when the absorbing and the photodesorbing molecules belong to different species during energy-transfer mediated processes, this mechanism is sometimes referred to as indirect DIET or photon-induced co-desorption, although no distinctions are made, in general.

³ Not to be confused with the kick-out photodesorption in van Hemert et al. (2015).

prior to the study of the photodesorption in more realistic multicomponent ice analogs. These studies have been reported for pure H₂O (Cruz-Díaz et al. (2017), and references therein), CO (Öberg et al. (2007, 2009b); Muñoz Caro et al. (2010); Fayolle et al. (2011); Bertin et al. (2012, 2013); Chen et al. (2014); Muñoz Caro et al. (2016)), CO₂ (Öberg et al. (2009b); Bahr & Baragiola (2012); Yuan & Yates (2013); Fillion et al. (2014); Martín-Doménech et al. (2015)), CH₃OH (Öberg et al. (2009a); Bertin et al. (2016); Cruz-Díaz et al. (2016)), CH₄ (Dupuy et al. (2017)), and NH₃ (Nishi et al. (1984); Loeffler & Baragiola (2010)) ices. In this work, we present a series of experiments simulating the UV photoprocessing of pure NH₃ ices focused on the subsequent photodesorption of ice molecules. Irradiation was carried out with a multiwavelength UV lamp, instead of a laser at a given wavelength used in Nishi et al. (1984); Loeffler & Baragiola (2010). In addition, we include the quantification of the different photodesorbing molecules measured directly from the gas phase, which was not reported in the previous works mentioned above, thanks to the calibration of the quadrupole mass spectrometer (QMS) used in our experimental setup (presented in Section 2) to detect the photodesorbing molecules. These results are presented in Section 3, and their astrophysical implications are discussed in Section 4. Finally, the conclusions are summarized in Section 5.

2 EXPERIMENTAL SETUP

The photodesorption of molecules from a pure NH₃ ice has been studied through a series of experimental simulations carried out with the InterStellar Astrochemistry Chamber (ISAC), an ultra-high-vacuum (UHV) setup located at the Centro de Astrobiología, with a working pressure of $\sim 4 \times 10^{-11}$ mbar, similar to that found in the interiors of dense interstellar clouds. A brief description of the experimental setup and the protocol followed during the experimental simulations is provided below (see Muñoz Caro et al. (2010); Martín-Doménech et al. (2015); Cruz-Díaz et al. (2016); Martín-Doménech et al. (2016) for more details). Pure amorphous ammonia ice samples were deposited from the gas phase onto a KBr window at 8 K used as the substrate, upon introduction of NH₃ (gas, Praxair 99.999%) into the chamber. The deposited ices were subsequently irradiated using an F-type microwave-discharged hydrogen flow lamp (MDHL) with a vacuum-ultraviolet (VUV) flux of 2×10^{14} photons cm⁻² s⁻¹ at the sample position (Muñoz Caro et al. (2010)). The total irradiation time varied between 60 and 1100 min, leading to the incident fluences indicated in Table 1. For a given fluence, the ice thickness determined the percentage of absorbed photons according to the VUV-absorption cross section reported in Cruz-Díaz et al. (2014a)⁴, as well as the incident and absorbed dose of photons per molecule. The results in Section 3 were not found to strongly depend on these parameters. The emission spectrum of the MDHL has been characterized in situ

⁴ The average absorption cross section of pure NH₃ ice is 6.1×10^{-18} cm² (Cruz-Díaz et al. (2014a)), which led to an absorption close to 100% of incident photons in most of the experiments (see Table 1).

Table 1. Experimental parameters of the UV photoprocessing of pure NH₃ ices

| Experiment | $N_{initial}(\text{NH}_3)$ ($\times 10^{15}$ molecules cm^{-2}) | Fluence _{incident} ($\times 10^{18}$ photons cm^{-2}) | Fluence _{absorbed} ^a ($\times 10^{18}$ photons cm^{-2}) | Dose _{incident} ^b (photons molecule ⁻¹) | Dose _{absorbed} ^a (photons molecule ⁻¹) | Heating rate (K/min) |
|------------|---|--|---|--|--|-------------------------|
| 1 | 237 | 2.16 | 1.32 | 9.11 | 5.58 | 2 |
| 2 | 835 | 2.88 | 2.78 | 3.45 | 3.33 | 2 |
| 3 | 912 | 2.88 | 2.80 | 3.16 | 3.07 | 2 |
| 4 | 913 | 0.72 | 0.70 | 0.79 | 0.77 | - |
| 5 | 1882 | 1.24 | 1.24 | 0.66 | 0.66 | - |
| 6 | 2264 | 13.27 | 13.27 | 5.86 | 5.86 | 2 |

^a The number of absorbed photons has been calculated taking into account the initial composition of the ice, i.e., the average UV absorption cross section for a pure NH₃ ice, provided by Cruz-Díaz et al. (2014a).

^b Relative to the initial number of NH₃ molecules.

using a VUV spectrophotometer, and is reported in Chen et al. (2010, 2014); Cruz-Díaz et al. (2014a). It is similar to the secondary UV field of dense cloud interiors calculated by Gredel et al. (1989). Finally, the ice samples in experiments 1-3 and 6 were warmed-up following irradiation to room temperature at a rate of 2 K/min.

During the experimental simulations, in situ Fourier-transform infrared (FTIR) transmittance spectroscopy was used to monitor the solid sample. IR spectra of the ices were collected after deposition, after every irradiation period, and every five minutes during warm-up, with a spectral resolution of 2 cm^{-1} . The initial column density N in molecules cm^{-2} of the NH₃ ices was calculated from the optical depth (τ_ν) of the N-H stretching absorption IR band at $\sim 3300 \text{ cm}^{-1}$, using the formula:

$$N = \frac{1}{A} \int_{band} \tau_\nu d\nu, \quad (1)$$

where A is the band strength in cm molecule^{-1} ($2.2 \times 10^{-17} \text{ cm molecules}^{-1}$; Schutte et al. (1996)). The ice thickness of the samples is usually expressed in monolayers (ML). One ML is assumed to be $10^{15} \text{ molecules cm}^{-2}$.

At the same time, all the desorbing species, including ammonia and the resulting products of the induced photochemical reactions, were detected in the gas phase by a Pfeiffer Prisma quadrupole mass spectrometer (QMS). The molecules reaching the QMS were ionized by $\sim 70 \text{ eV}$ electron bombardment, which led to fragmentation following a given pattern. The main mass fragments coincided in this case with the molecular ions, and were used to monitor the presence of NH₃ ($m/z = 17$), and the photoproducts N₂ ($m/z = 28$), H₂ ($m/z = 2$), and N₂H₄ ($m/z = 32$) in the gas phase. The conversion from the integrated ion currents measured by the QMS for every irradiation period ($A(m/z)$) into photodesorbing column densities ($N(mol)$) was carried out using the equation:

$$N(mol) = \frac{A(m/z)}{k_{CO}} \cdot \frac{\sigma^+(CO)}{\sigma^+(mol)} \cdot \frac{I_F(CO^+)}{I_F(z)} \cdot \frac{F_F(28)}{F_F(m)} \cdot \frac{S(28)}{S(m/z)}. \quad (2)$$

The meaning of the different parameters in Eq. 2 is described in Martín-Doménech et al. (2015); Cruz-Díaz et al. (2016); Martín-Doménech et al. (2016); Cruz-Díaz et al. (2017). The values used in this work are summarized in Table 2, and in the text. The constant k_{CO} and the sensitivity of

the QMS are regularly calibrated (see Martín-Doménech et al. (2015) for more information on the calibration process).

Since the pumping speeds in the ISAC setup are not the same for all molecules, $N(mol)$ from Eq. 2 must be corrected to take into account the different pumping speed of the species of interest with respect to the CO molecules used as reference to extract k_{CO} :

$$N^{real}(mol) = N(mol) \cdot S_{rel}(mol), \quad (3)$$

where the relative pumping speed ($S_{rel}(mol)$) can be calculated as

$$S_{rel}(mol) = 1.258 - 9.2 \cdot 10^{-3} \cdot M(mol), \quad (4)$$

(see Kaiser et al. (1995); Martín-Doménech et al. (2016) for more information). Photodesorption yields are finally calculated dividing $N^{real}(mol)$ by the fluence.

3 EXPERIMENTAL RESULTS AND DISCUSSION

3.1 Photon-induced chemistry of pure NH₃ ice

3.1.1 IR spectra of NH₃ ice during irradiation

The IR spectrum of a pure and amorphous NH₃ ice presents three different features: a wide band centered at $\sim 3300 \text{ cm}^{-1}$ (see black curve in left panel of Fig. 1) corresponding to the N-H stretching modes (the symmetric mode peaks at $\sim 3375 \text{ cm}^{-1}$, and the antisymmetric mode at $\sim 3200 \text{ cm}^{-1}$); a weaker band at $\sim 1625 \text{ cm}^{-1}$ (see black curve in right panel of Fig. 1) corresponding to the N-H bending mode; and a third band at 1070 cm^{-1} (not shown) corresponding to the so-called umbrella mode. During photoprocessing of pure NH₃ ices, photodissociation and photodesorption of the NH₃ molecules decrease the absorbance of these bands, as shown in Fig. 1 for the former two features.

Photodissociation in the gas phase of NH₃ molecules readily leads to the formation of NH₂ and NH radicals due to the loss of one or two hydrogen atoms, respectively, although the formation of ground-state NH radicals is spin-forbidden (Okabe (1978)). Formation of NH₂ during irradiation of pure NH₃ ice was reported in Gerakines et al. (1996) and Loeffler & Baragiola (2010) thanks to an IR peak detected above 1500 cm^{-1} on the red wing of the NH₃ bending

Table 2. Values of the parameters in Eq. 2 used to convert integrated QMS signals into photodesorbing column densities. Photodesorbing H₂ was not quantified due to contamination issues (see text).

| Factor | NH ₃ | N ₂ | CO |
|---|--|-----------------------------|-------------------------|
| σ^+ (mol) (angstroms ²) ^a | 3.036 | 2.508 | 2.516 |
| fragment | NH ₃ ⁺ | N ₂ ⁺ | CO ⁺ |
| m/z | 17 | 28 | 28 |
| $I_F(z)$ | 1 ^b | 1 ^b | 1 ^b |
| $F_F(m)$ | 0.460 ^c 0.514 ^d 0.498 ^e | 0.933 ^a | 0.949 ^a |
| $k_{QMS}^* \cdot S(m/z)^5$ (A mbar ⁻¹ - ²) | 1.78 x 10 ¹⁵ | 1.03 x 10 ¹⁵ | 1.03 x 10 ¹⁵ |
| $S_{rel}(mol)^f$ | 1.1 | 1.0 | 1.0 |

^a Extracted from the online database of the National Institute of Standard and Technologies (NIST).

^b We assumed that no double ionization of the molecules took place in the QMS.

^c Calculated during the deposition in experiment 1

^d Calculated during the deposition in experiments 2,3,4, and 6

^e Calculated during the deposition in experiment 5

^f Calculated with equation 3.

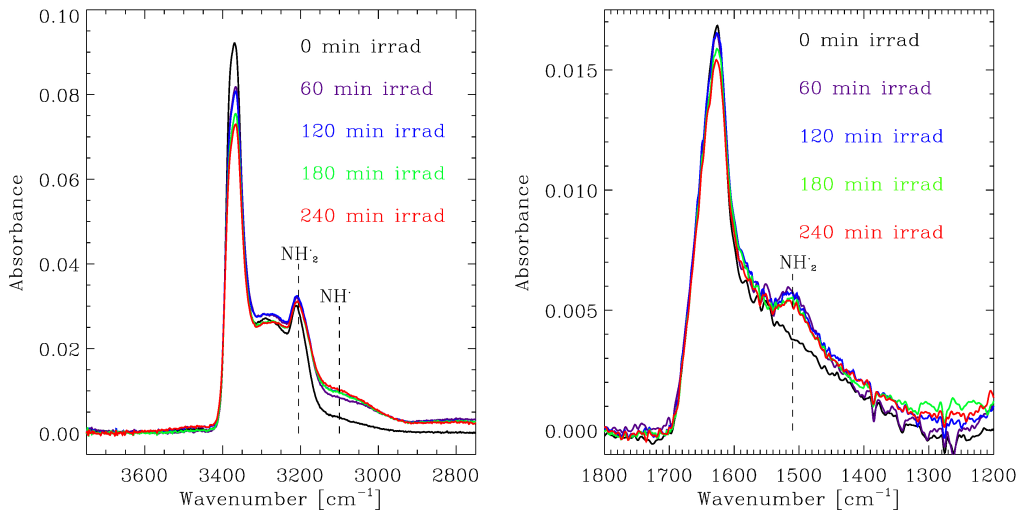


Figure 1. IR spectra of the ice sample after every irradiation interval during photoprocessing in experiment 3 (see Table 1). Similar results were found for the rest of the experiments. *Left:* IR band corresponding to the N-H stretching modes of the NH₃ molecules. The decrease in the IR absorbance is due to the photodissociation and photodesorption of NH₃ molecules during irradiation. The weak shoulder above 3000 cm⁻¹ corresponds to the N-H stretching mode of the NH[·] radical. *Right:* IR band corresponding to the N-H bending mode of the NH₃ molecules (smoothed). The peak observed at ~1500 cm⁻¹ corresponds to the formation of the NH₂ radical.

band. This peak is observed in the right panel of Fig. 1. In addition, a decrease in the intensity ratio between the symmetric and antisymmetric N-H stretching modes in the left panel of Fig. 1 is probably due to the contribution of the absorption corresponding to the antisymmetric N-H stretching mode of NH₂ (Milligan & Jacox (1965)). At the same time, a wide shoulder at ~3100 cm⁻¹ on the red wing of the N-H stretching band shown in the left panel of Fig. 1 could be attributed to the imidogen radical (NH[·]; Rosengren & Pimentel (1965)). During the warm-up phase of the experiment, after photoprocessing of the ice sample is complete, the mobility of these radicals is increased. Diffusion and subsequent reaction of the radicals led to a decrease of their IR

features. The IR peak at ~1500 cm⁻¹ corresponding to the bending mode of the NH₂ radical, disappears between 26 K and 73 K, as shown in the right panel of Fig. 2. At 67 K, the intensity of this feature is roughly half of that at 8 K, and has completely disappeared at 73 K. In addition, a slight decrease in the shoulder at ~3100 cm⁻¹ corresponding to the imidogen radical is observed at temperatures above 67 K (left panel of Fig. 2).

During irradiation, NH[·] and NH₂ radicals can be dissociated by subsequent photons leading to the production of H and N atoms, that recombine to form H₂ and N₂ molecules (see Loeffler & Baragiola (2010), where additional pathways to the formation of these photoproducts are reported), which

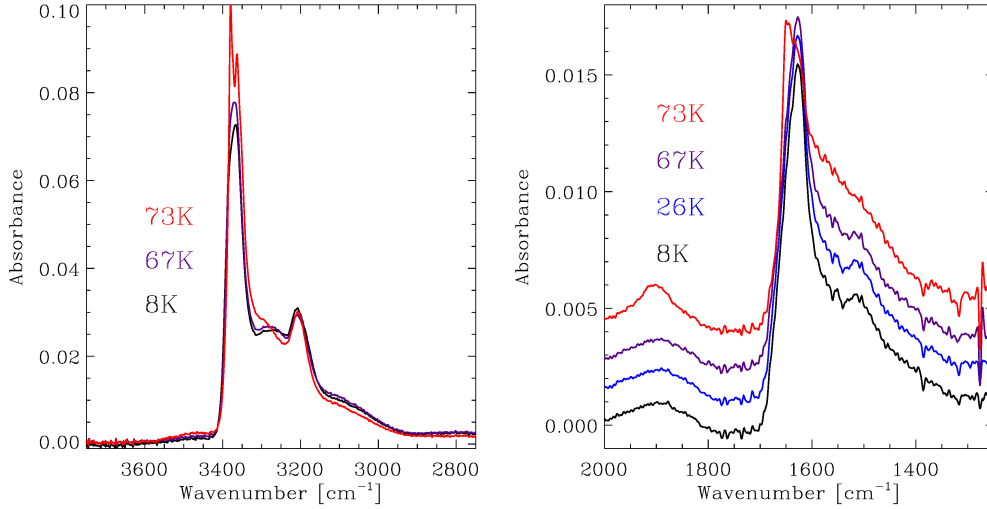


Figure 2. IR spectra of the ice sample during the temperature-programmed desorption after irradiation in experiment 3 (see Table 1). Similar results were found for the rest of experiments. *Left:* Above 67 K, a change in the NH₃ ice matrix structure leads to a change in the N-H stretching band profile (see also Satorre et al. (2013), Giuliano et al. (2014)). At the same time, the shoulder above 3000 cm⁻¹ slightly decreases, probably due to the diffusion and subsequent reactions of the NH[•] radical. *Right:* Above 26 K, the intensity of the peak corresponding to the NH₂ radical also decreases due to its diffusion and subsequent reactions, and has completely disappeared at a temperature of 73 K, indicating that no free radicals are left in the ice sample at that temperature. Spectra are shifted for clarity.

are IR inactive due to the lack of an electric dipole moment. Formation of these molecules is confirmed thanks to the temperature-programmed desorption (TPD) of the irradiated ices during the warm-up phase of the experiments (see Sect. 3.1.2). In addition, formation of hydrazine (N₂H₄) by recombination of two NH₂ radicals, or reaction of a NH[•] radical with a NH₃ molecule (Loeffler & Baragiola (2010)), is also reported at a temperature of 10 K in Gerakines et al. (1996). Although no IR absorption corresponding to this molecule was detected during our experimental simulations, formation of this molecule was also confirmed during the TPD of the irradiated ices (Sect. 3.1.2).

3.1.2 Temperature-programmed desorption of the irradiated NH₃ ice

After photoprocessing of the ice samples, a constant heating rate was applied to perform the TPD of the irradiated ices. Thermal desorption of ammonia and the photoproducts H₂, N₂, and N₂H₄ was detected by the QMS at a given temperature according to their volatility, as shown in Fig. 3. In particular, desorption of H₂ molecules was observed at a wide range of temperatures, since the very beginning of the warm-up phase of the experiment, due to the high volatility of this species. A desorption peak corresponding to most of the photoproducted N₂ molecules was observed at 29 K (slightly higher than the desorption temperature reported in Fayolle et al. (2016) for pure N₂ ices, probably due to the effect of the NH₃ matrix). On the other hand, the hydrazine molecules finally desorbed at 172 K, a desorption temperature 10-20 K lower than that reported in Roux & Wood (1983) for experiments performed in a high-vacuum chamber with a base pressure five orders of magnitude higher compared to the one in the ISAC setup.

3.2 Photodesorption from pure NH₃ ice

During irradiation of the ice samples, the photodesorbing molecules were detected in the gas phase by the QMS. In particular, photodesorption led to an increase on the signal of the m/z fragments of the photodesorbing molecules during every irradiation interval. The measured ion current of the main mass fragments corresponding to NH₃ (m/z = 17), and the three photoproducts: H₂ (m/z = 2), N₂ (m/z = 28), and N₂H₄ (m/z = 32), are shown in Fig. 4. Photodesorption of the former three species was detected, as in Nishi et al. (1984) and Loeffler & Baragiola (2010), while N₂H₄ was not found to photodesorb. The integrated QMS ion currents were converted into photodesorbing column densities using Equations 2 and 3, the parameter values shown in Table 2, and a $k_{CO} = 5.55 \times 10^{-12}$ A min ML⁻¹. The ratio of the photodesorbing column densities in every irradiation period and the incident fluence during the same period led to the average photodesorption yield for every irradiation interval shown in Table 3. Quantification of the photodesorbing H₂ molecules was not included since the measured values suffered from background H₂ contamination, which is the most usual contaminant in UHV chambers.

Photodesorption of NH₃ molecules took place with an average photodesorption yield of $2.1 \times 10^{-3} \frac{\text{molecules}}{\text{incident photon}}$, that remained constant during the whole experiment (see Table 3). This is similar, within errors, to the photodesorption yield indirectly measured in the solid phase by Loeffler & Baragiola (2010) with a quartz-crystal microbalance (QCM)⁶ during photoprocessing of a pure NH₃ ice grown at 40 K using a 193 nm ArF laser.

During irradiation of pure ice samples, it is not possible

⁶ The QCM measured the total ice mass loss, which was assigned mostly to ejected NH₃ molecules, although it included any other photodesorbing product.

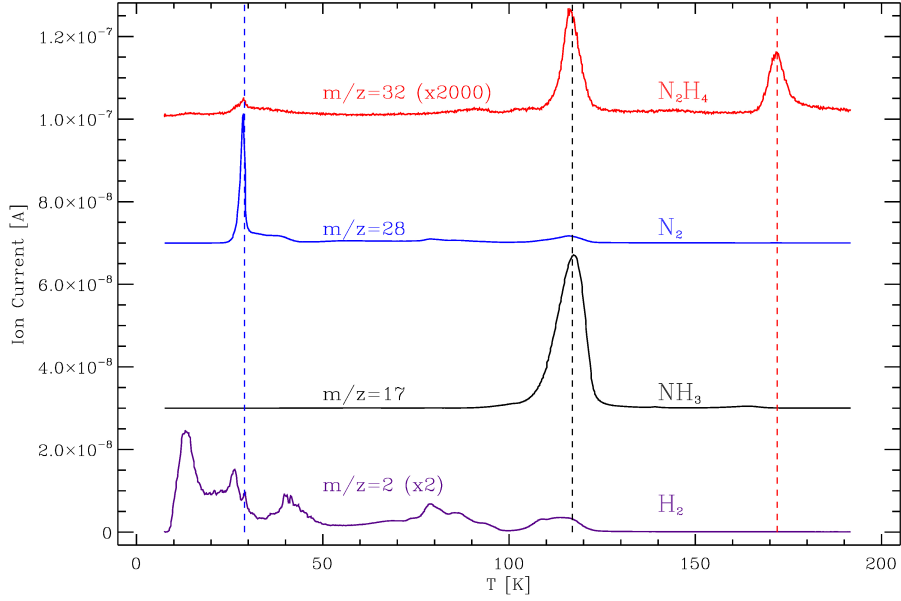


Figure 3. Thermal desorption peaks detected by the QMS for different m/z fragments during the TPD phase of experiment 6 (see Table 1, similar results were found for the rest of experiments) corresponding to NH_3 ($m/z=17$, black) and the three irradiation products: H_2 ($m/z=2$, purple), N_2 ($m/z=28$, blue), and N_2H_4 ($m/z=32$, red). TPD curves are shifted for clarity. The desorption peak observed for $m/z=32$ at $T = 117$ K is probably due to an ion-molecule reaction of ammonia inside the mass spectrometer, since it is also observed in experiments with no ammonia-ice irradiation.

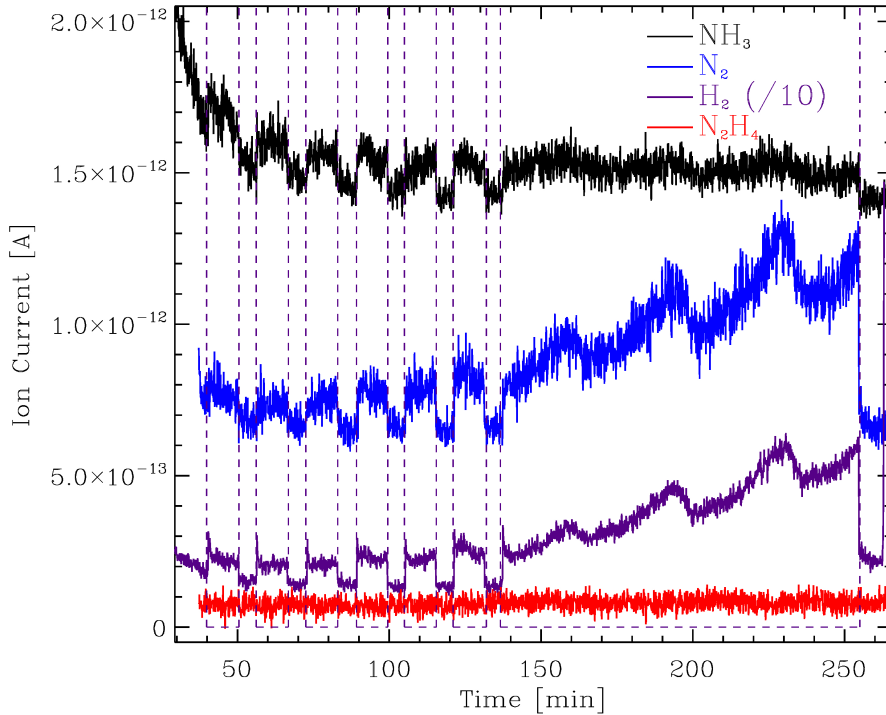


Figure 4. Photodesorption of NH_3 (black), and the photoproducts H_2 (purple) and N_2 (blue) detected by the QMS during irradiation of the ice sample in experiment 1 (see Table 1, similar results were found for the rest of experiments). Irradiation intervals are indicated with vertical dashed lines. The increase in the photodesorption of H_2 and N_2 suggests that these molecules photodesorb mainly through an indirect mechanism (see text), while the photoproduct N_2H_4 (red) was not found to photodesorb. Signals are shifted for clarity. Fluctuations in the signals are due to instabilities on the VUV flux during long irradiation periods.

Table 3. Photodesorption yields measured for the different irradiation intervals during photoprocessing of a pure NH₃ ice in experiment 1, see Table 1. Similar results were found for experiments 2-6.

| Irradiation period (min) | Fluence ^a × 10 ¹⁷ (photons cm ⁻²) | Y_{pd} (NH ₃) ^b × 10 ⁻³ | Y_{pd} (N ₂) ^b ($\frac{\text{molecules}}{\text{incident photon}}$) |
|-----------------------------|--|--|--|
| 0 - 10 | 1.2 | 2.05 | 1.51 |
| 10 - 20 | 2.4 | 2.12 | 1.36 |
| 20 - 30 | 3.6 | 1.89 | 2.18 |
| 30 - 40 | 4.8 | 2.28 | 2.41 |
| 40 - 50 | 6.0 | 1.92 | 2.64 |
| 50 - 60 | 7.2 | 2.01 | 3.05 |
| 60 - 180 | 21.6 | 1.74 | 5.86 |

^a Total fluence at the end of every irradiation period.

^b Averaged for every irradiation period. A factor of 2 is assumed as the error in the photodesorption yield values due to the uncertainties in all the parameters of equation 2 (see also Martín-Doménech et al. (2016)).

to elucidate whether photodesorption of the original ice component takes place through a direct mechanism or through a mechanism involving energy transfer attending only to the evolution of the photodesorption yield with fluence. This can only be done for the photodesorption of photoproducts, as explained in Sect. 1. Nishi et al. (1984) measured the energy distribution of the photodesorbing NH₃ molecules from a pure NH₃ ice grown at 90 K and irradiated with a 193 nm ArF laser, using a time-of-flight (TOF) mass spectrometer. Two energy components with mean translational energies of 0.17 eV and 0.65 eV, respectively, were found. The low energy component was associated to NH₃ molecules photodesorbing through a mechanism involving energy transfer from the absorbing molecule in the bulk of the ice to a surface molecule. This is similar to the DIET mechanism involving energy transfer described in Sect. 1. In this case, absorption of a photon led to a transition to a Wannier exciton state that subsequently propagated through the crystal approaching a weakly bound edge molecule that acquired linear momentum due to the electronic repulsive force. On the other hand, the high energy component, that accounted for half of the photodesorbing molecules, was associated to excited surface molecules, probably desorbing after recombination of a previously photodissociated NH₃ molecule.

Photodesorption of H₂ and N₂ molecules took place with an increasing photodesorption yield with fluence, as reported in Loeffler & Baragiola (2010). The photodesorption yield of N₂ was found to be $1.4 \times 10^{-3} \frac{\text{molecules}}{\text{incident photon}}$ (i.e., on the order of that of NH₃) for a fluence of up to 2.4×10^{17} photons cm⁻², and then gradually raised, being ~4 times higher when the total fluence was 2.2×10^{18} (see Table 3). In this case, the increasing photodesorption yield is related to the accumulation of photoproducted H₂ and N₂ molecules in the ice sample prior to their desorption into the gas phase. Therefore, there is a significant contribution of indirect photodesorption mechanisms involving energy transfer. These mechanisms require the absorption of a new photon after the formation of the photoproducts, as explained in Sect. 1, in contrast to the direct photodesorption mechanisms where desorption occurs immediately after the formation of the molecules, without the need of absorbing a new photon. In that case, the photoproduct molecules could not accumulate on the surface of the ice before their desorption, leading to

a constant photodesorption yield with fluence (see Martín-Doménech et al. (2015, 2016); Cruz-Díaz et al. (2016, 2017)).

4 ASTROPHYSICAL IMPLICATIONS

Ammonia ice is thought to form early at the onset of the diffuse cloud collapse that leads to the formation of dense clouds where ice mantles are usually detected, by hydrogenation reactions of N atoms on the surface of dust grains. The abundance of NH₃ with respect to H₂O in the ice mantles is around 5% in dense clouds and also in the cold circumstellar envelopes around protostars (see Boogert et al. (2015), and references therein). Its importance, though, is beyond all doubts since it is the only confirmed source of N atoms in interstellar ices. The detection of ammonia in the gas-phase of the cold ISM was already reported in Cheung et al. (1968).

NH₃ ice molecules are photoprocessed along with all the ice components in the interior of dense clouds thanks to the secondary UV field mentioned in Sect. 1, leading to photochemical reactions that produce new ice molecules and photodesorption processes that allow the presence of molecules in the gas phase of cold interstellar regions where thermal desorption is negligible. These processes can be simulated in the laboratory under astrophysically relevant conditions. For the VUV flux of the lamp used (see Sect. 2), the ice samples experience a fluence of $\sim 3 \times 10^{17}$ photons cm⁻² after ~30 minutes of irradiation in our experiments, which is similar to the fluence experienced by the ice mantles during the expected lifetime of a molecular cloud, assuming a secondary UV flux of $\sim 10^4$ photons cm⁻² s⁻¹ (Shen et al. (2004)). The six components confirmed to be present in the interstellar ices are distributed over two distinct ice layers as the result of the formation process (see Boogert et al. (2015), and references therein). A polar ice layer is formed first on the surface of dust grains, dominated by H₂O and including NH₃, CH₄, and a fraction of the CO₂ ice molecules. On top of this polar ice layer, an apolar layer is subsequently formed, mainly composed by CO along with the rest of the CO₂ molecules and probably CH₃OH. In any case, irradiation experiments of pure ices are used as benchmarks in the study of the photoprocessing of more realistic multicomponent ices.

In our experimental simulations using a MDHL, whose

Table 4. Photodesorption yields measured for pure ices during irradiation with a MDHL.

| Ice component | Y_{pd} $\times 10^{-3}$ ($\frac{\text{molecules}}{\text{incident photon}}$) | Reference |
|--------------------|--|-------------------------------|
| H ₂ O | 1.3 ± 0.2 | Cruz-Díaz et al. (2017) |
| CO | 54.0 ± 5.0 | Muñoz Caro et al. (2010) |
| CO ₂ | 0.1 ± 0.04 | Martín-Doménech et al. (2015) |
| CH ₃ OH | ≤ 0.03 | Cruz-Díaz et al. (2016) |
| NH ₃ | $2.0^{+2.1}_{-1.0}$ | This work |

emission spectrum is similar to that expected in the interior of dense clouds, photodesorption of NH₃ molecules is observed to proceed with a constant yield with fluence during irradiation of a pure NH₃ ice ($Y_{pd}(\text{NH}_3) = 2.1^{+2.1}_{-1.0} \times 10^{-3} \frac{\text{molecules}}{\text{incident photon}}$). This value is on the order of the observed H₂O photodesorption during photoprocessing of pure H₂O ices using the same UV lamp, (Cruz-Díaz et al. (2017)), while it is one order of magnitude lower than the photodesorption yield of CO molecules during photoprocessing of a pure CO ice (Muñoz Caro et al. (2010)), and one order of magnitude higher than that measured for CO₂ (see Table 4) under similar conditions (Martín-Doménech et al. (2015)). Photodesorption of NH₃ molecules from an ice mixture dominated by water will be addressed in a forthcoming paper, and is expected to be lower than the value presented in this paper for segregated (pure) NH₃ ice (Loeffler & Baragiola (2010)).

On the other hand, we also observed photodesorption of the produced N₂ molecules, with a yield that increased for fluences higher than 2.4×10^{17} photons cm⁻². For a fluence similar to that experienced by the ice mantles in the expected lifetime of a dense cloud ($\sim 3 \times 10^{17}$ photons cm⁻²), the average photodesorption yield of N₂ molecules was similar to that observed for the NH₃ molecules ($Y_{pd}(\text{N}_2) = 1.7^{+1.7}_{-0.9} \times 10^{-3} \frac{\text{molecules}}{\text{incident photon}}$). Photodesorption of N₂ molecules from a pure N₂ ice is expected to be negligible, due to the low VUV-absorption cross section of this ice (the average absorption cross section is 7.0×10^{-21} cm², while for NH₃ ices it is 6.1×10^{-18} cm²; Cruz-Díaz et al. (2014a,b)). Detection of gas-phase N₂ was reported in Knauth et al. (2004) from far-UV observations toward the star HD 124314, with an abundance that could not be explained with gas-phase chemical models for either diffuse or dense clouds.

5 CONCLUSIONS

We have performed experimental simulations of the UV photoprocessing of NH₃ ice using a MDHL with an emission spectrum similar to that expected to be present in the interior of dense clouds. IR spectroscopy in transmittance was used to monitor the solid sample during irradiation. Formation of NH₂ and NH⁻ radicals due to the photodissociation of NH₃ molecules was observed thanks to the appearance of IR features at ~ 1500 cm⁻¹ and ~ 3100 cm⁻¹, respectively. The photoproducts H₂ and N₂ are not IR active, and the N₂H₄ IR features did not reach the sensitivity limit in the spectra of the irradiated ices, but they were detected in the gas phase after thermal desorption during the TPD of the photoprocessed ice thanks to a QMS.

In addition, photodesorption of NH₃ and the photo-products H₂ and N₂ were detected by the QMS during photoprocessing of the ice samples. Photodesorption of NH₃ took place with a constant yield with fluence, as it is the case for other species during irradiation of their pure ices. On the other hand, the photodesorption yield of H₂ and N₂ were observed to increase with fluence, pointing toward a significant contribution of indirect photodesorption mechanism involving energy transfer from the absorbing molecule to a previously formed H₂ or N₂ molecule, that subsequently desorbed. This kind of mechanism allows accumulation of the photoproducts prior to their desorption, leading to an increase of the number of molecules available for the photodesorption and, therefore, an increase of the photodesorption yield with fluence.

The calibration of the QMS allowed us to quantify the photodesorption yields for the desorbing molecules. NH₃ molecules were found to photodesorb with an average yield of $2.1^{+2.1}_{-1.0} \times 10^{-3} \frac{\text{molecules}}{\text{incident photon}}$, which is of the same order than the photodesorption measured for H₂O molecules during irradiation of a pure water ice (Cruz-Díaz et al. (2017)). N₂ molecules are not expected to efficiently photodesorb from pure N₂ ices ($Y_{pd}(\text{N}_2) \leq 2 \times 10^{-4} \frac{\text{molecules}}{\text{incident photon}}$; Öberg et al. (2009b)), probably due to their low VUV-absorption cross section (Cruz-Díaz et al. (2014b)). During irradiation of a pure NH₃ ice, a photodesorption yield similar to that of NH₃ molecules was measured for N₂ molecules, for a fluence equivalent to that experienced by ice mantles during the expected lifetime of dense clouds ($Y_{pd}(\text{N}_2) = 1.7^{+1.7}_{-0.9} \times 10^{-3} \frac{\text{molecules}}{\text{incident photon}}$), although photodesorption yields up to four times higher were measured for higher fluences.

ACKNOWLEDGMENTS

This research was financed by the Spanish MINECO under projects AYA2011-29375 and AYA2014-60585.

REFERENCES

- Andersson, S., & van Dishoeck, E.F. 2008, A&A, 491, 907
- Bahr, D.A., Baragiola, R.A. 2012, ApJ, 761, 1, id.36
- Bergin, E.A., Ciardi, D.R., Lada, C.J., Alves, J., & Lada, E.A. 2001, ApJ, 557, 209
- Bertin, M., Fayolle, E. C., Romanzin, C., Öberg, K.I., Michaut, X., et al. 2012, PCCP, 14, 9929
- Bertin, M., Fayolle, E. C., Romanzin, C., Ponderoso, H.A.M., Michaut, X., et al. 2013, ApJ, 779, 120
- Bertin, M., Romanzin, C., Doronin, M., Philippe, L. Jeseck, P., et al. 2016, ApJL, 817, 2, L12

- Boogert, A.C.A., Gerakines, P.A., & Whittet, D.C.B. 2015, *ARA&A*, 53, 541
- Cecchi-Pestellini, C., & Aiello, S. 1992, *MNRAS*, 258, 125
- Chen, Y.-J., Chu, C.-C., Lin, Y.-C. et al. 2010, *Advances in Geosciences*, 25, 259
- Chen, Y.-J., Chuang, K.-J., Muñoz Caro, G. M., Nuevo, M., Chu, C.-C., et al. 2014, *ApJ*, 781, 15
- Cheung, A.C., Rank, D.M., Townes, C.H., Thornton, D.D., & Welch, W.J. 1968, *Phys. Rev. Lett.* 21, 1701
- Cruz-Díaz, G.A., Martín-Doménech, R., Muñoz Caro, G.M., & Chen, Y.-J. 2016, *A&A*, 592, A68
- Cruz-Díaz, G.A., Martín-Doménech, R., Moreno, E. Muñoz Caro, G.M., & Chen, Y.-J. 2017, *submitted*
- Cruz-Díaz, G.A., Muñoz Caro, G.M., Chen, Y.-J., & Yih, T.-S. 2014a, *A&A*, 562, A119
- Cruz-Díaz, G.A., Muñoz Caro, G.M., Chen, Y.-J., & Yih, T.-S. 2014b, *A&A*, 562, A120
- Dupuy, R., Bertin, M., Féraud, G., Michaut, X., Jeseck, P., et al. 2017, *A&A*, 603, A61
- Fayolle, E., Balfe, J. Loomis, R., Bergner, J., Graninger, D., et al. 2016, *ApJL*, 816, 2, L28
- Fayolle, E., Bertin, M., Romanzin, C., Michaut, X., Öberg, K., et al. 2011, *ApJL*, 739, L36
- Fayolle, E., Bertin, M., Romanzin, C., Poderoso, H.A.M., Philippe, L., et al. 2013, *A&A*, 556, A122
- Fillion, J.-H., Fayolle, E., Michaut, X., Doronin, M., Philippe, L., et al. 2014, *Faraday Discuss.*, 168, 533
- Gerakines, P.A., Schutte, W.A., & Ehrenfreund, P. 1996, *A&A*, 312, 289
- Gibb, E.L., Whittet, D.C.B., Boogert, A.C.A., & Tielens, A.G.G.M. 2004, *ApJSS*, 151, 35
- Giuliano, B.M., Escribano, R.M., Martín-Doménech, R. Dartois, E., & Muñoz Caro, G.M., 2014, *A&A*, 565, A108
- Gredel, R., Lepp, S., Dalgarno, A., & Herbst, E. 1989, *ApJ*, 347, 289
- Kaiser, R. I., Jansen, P., Petersen, K., & Roessler, K. 1995, *Rev. Sci. Instrum.* 66, 5226
- Knauth, D.C., Anderson, B.-G., McCandliss, S.R., & Moss, H.W. 2004, *Nature*, 429, 636
- Loeffler, M.J., & Baragiola, R.A. 2010, *J. Chem. Phys.*, 133, 214506
- Martín-Doménech, R., Manzano-Santamaría, J., Muñoz Caro, G.M., Cruz-Díaz, G.A., Chen, Y.-J., et al. 2015, *A&A*, 584, A14
- Martín-Doménech, R., Muñoz Caro, G.M., & Cruz-Díaz, G.A. 2016, 589, A107
- Milligan, D.E. & Jacox, M.E. 1965, *J. Chem. Phys.*, 43, 12, 4487
- Muñoz Caro, G. M., Chen, Y.-J., Aparicio, S., Jiménez-Escobar, A., Rosu-Finsen, A., et al. 2016, *A&A*, 589, A19
- Muñoz Caro, G. M., Jiménez-Escobar, A., Martín-Gago, J.Á. et al. 2010, *A&A*, 522, A108
- Nishi, N., Shinohara, H., & Okuyama, T. 1984, *J. Chem. Phys.*, 80, 3898
- Öberg, K.I. 2016, *Chem. Rev.*, 116 (17), 9631
- Öberg, K.I., Boogert, A.C.A., Pontoppidan, K.M., van den Broek, S., van Dishoeck, E.F., et al. 2011, *ApJ*, 740, 109
- Öberg, K.I., Fuchs, G.W., Awad, Z., Fraser, H., Schlemmer, S., et al. 2007, *ApJL*, 662, L23
- Öberg, K.I., Garrod, R.T., van Dishoeck, E.F., & Linnartz, H. 2009, *A&A*, 504, 3, 891
- Öberg, K.I., van Dishoeck, E.F., & Linnartz, H. 2009, *A&A* 496, 281
- Okabe, H. 1978, *Photochemistry of small molecules*, ed. John Wiley & Sons, New York
- Rosengren, K., & Pimentel, G.C. 1965, *J. Chem. Phys.*, 43, 2, 507
- Roux, J.A., & Wood, B.E. 1983, *J. Opt. Soc. Am.*, 73, 9, 1181
- Satorre, M.Á., Leliwa-Kopystynski, J., Satonja, C., & Luna, R. 2013, *Icarus*, 225, 1, 703
- Schutte, W. A., Gerakines, P. A., Geballe, T. R., van Dishoeck, E. F., & Greenberg, J. M. 1996, *A&A*, 309, 633
- Shen, C.J., Greenberg, J.M., Schutte, W.A., & van Dishoeck, E.F. 2004, *A&A*, 415, 203
- van Hemert, M.C., Takahashi, J., & van Dishoeck, E.F. 2015, *J. Chem. Phys. A*, 119, 24, 6354
- Wilacy, K., & Langer, W.D. 2000, *ApJ*, 544, 903
- Yuan, C., & Yates, J.T. 2013, *J. Chem. Phys.*, 138, 15, 154303

This paper has been typeset from a $\text{\TeX}/\text{\LaTeX}$ file prepared by the author.